Applied Nanoscience (2023) 13:6905–6918
https://doi.org/10.1007/s13204-023-02801-w

ORIGINAL ARTICLE

Fast synthesis of $MgO–Al_2O_3$ systems: effect on physicochemical characteristics and catalytic properties in Guerbet condensation of ethanol

Karina V. Valihura[1,2] · Olga V. Larina[1] · Pavlo I. Kyriienko[1] · Pavlo S. Yaremov[1] · Ivan Khalakhan[3] · Volodymyr V. Trachevskiy[4] · Sergiy O. Soloviev[1] · Svitlana M. Orlyk[1]

Received: 14 December 2022 / Accepted: 10 February 2023 / Published online: 21 March 2023

Abstract

A series of hydrotalcite-derived Mg–Al oxide systems with Mg/Al atomic ratios of 2 and 3 were synthesized. The hydrotalcite of Mg–Al-2 and Mg–Al-3 samples was prepared for 24 h, and Mg–Al-2-Fast and Mg–Al-3-Fast samples were kept only for 1 h. The physicochemical characteristics of the samples were studied by X-ray diffraction, scanning electron microscopy, and ^{27}Al nuclear magnetic resonance. The surface area of the samples was determined by low-temperature N_2 ad(de)sorption at 77 K. NH_3 and CO_2 temperature-programmed desorption was applied to determine the acid and base sites of the surface. Based on the study of Mg–Al oxide samples with different times of hydrotalcite preparation, it was found that reducing the maturation time of the mother liquor after coprecipitation from 24 to 1 h increased the volume and the surface area of mesopores and external specific area of the samples, and also the concentration of weak and medium weak base sites. These in turn increase the activity of the catalysts and the selectivity of 1-butanol formation in the process of Guerbet condensation of ethanol. The highest 1-butanol selectivity of 64% and the yield of 23.4% are achieved over the Mg–Al-2-Fast catalyst at 548 K (with stable selectivity of 64% up to 12 h).

Keywords Fast synthesis · $MgO–Al_2O_3$ systems · Hydrotalcite-derived materials · Physicochemical characteristics · Catalytic properties · Guerbet condensation of ethanol

Introduction

1-Butanol (BuOH) is traditionally used in the production of polymers, synthetic rubber, brake fluids, lubricants, and solvents, and also as an intermediate to obtain such important chemicals as acetates, acrylate esters, amines, amino resins, butyl acrylate, glycol ether, and methacrylate (Choi et al. 2021). In addition, 1-butanol was proposed as a more desirable transportation blend fuel compared to ethanol (EtOH) because of its significantly higher energy content, better miscibility with ordinary gasoline, lower miscibility with water, and lower corrosion activity (Trindade and Santos 2017; Nair and Meenakshi 2021).

Nowadays, the main amount of 1-butanol is still produced using a petrochemical reaction (Daramola and Ayeni 2020) through propene hydroformylation with subsequent hydrogenation of the aldehydes formed (Hahn et al. 2013). Another commercial approach to produce BuOH consists of microbial fermentation of starchy and sugar feedstock, which provides a mixture of acetone, 1-butanol, and ethanol (ABE fermentation) (Birgen et al. 2019). The main issues in the biosynthesis development of 1-butanol are the high cost of fermentation substrate and the low concentration of bio-butanol fermentation broth which is limited by the toxic metabolic products in the fermentation process. 1-Butanol synthesized from biomass-derived ethanol can

✉ Karina V. Valihura
karina.valigura@ukr.net

1 L.V. Pisarzhevskii Institute of Physical Chemistry of the National Academy of Sciences of Ukraine, 31 Prosp. Nauky, Kyiv 03028, Ukraine

2 Departamento de Ingeniería Química y Ambiental, Escuela Técnica Superior de Ingeniería, Universidad de Sevilla, Camino de los Descubrimientos s/n, 41092 Seville, Spain

3 Faculty of Mathematics and Physics, Charles University, V Holešovičkách 2, 18000 Prague, Czech Republic

4 Institute for Sorption and Problems of Endoecology of the National Academy of Sciences of Ukraine, 13 Henerala Naumova St., Kyiv 03164, Ukraine

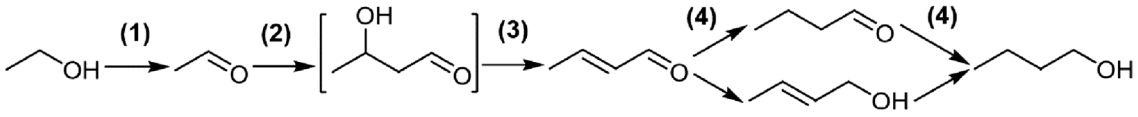

Scheme 1 Guerbet reaction mechanism: 1-dehydrogenation of initial alcohol to aldehyde, 2-aldol self-condensation of aldehyde, 3-dehydration of the aldol product to unsaturated aldehyde, 4-hydrogenation and/or Meerwein-Ponndorf-Verley reduction of the unsaturated aldehyde into resulting alcohol

serve as a replacement for petroleum-derived products (Choudhary et al. 2022).

Alcohol coupling, also known as the Guerbet reaction, is a C–C bond formation that involves the coupling of two alcohol molecules through a complex reaction sequence (Liu et al. 2021): (1) dehydrogenation, (2) aldol condensation, (3) dehydration, and (4) hydrogenation/reduction. This process leads to the carbon chain elongation and can be described by the following (Scheme 1).

This leads to clear design considerations when developing the catalysts: catalysts should possess (1) the ability to facilitate the dehydrogenation of alcohols and (2) the capacity for aldol condensation (Wu et al. 2021).

Metal oxides, in particular, $MgO–Al_2O_3$, metal phosphates, and supported transition metals, are important components of heterogeneous catalysts for the process (Gabriëls et al. 2015; Wu et al. 2018; Dai and Zhang 2019). It was found that the Mg/Al ratio of Mg–Al-oxide catalysts and acid–base characteristics has an effect on a yield of the target product in vapor phase Guerbet condensation of (bio)alcohols in a flow reactor (Larina et al. 2019; Valihura et al. 2019). Thus, the major challenge for the further development and application of the ethanol-to-1-butanol conversion process is to find an optimal ratio between acid/base characteristics of the catalyst, which can be made by variable preparation method. Park et al. (Park et al. 2019) concluded that the preparation method strongly affected the structure of Mg–Al hydrotalcite, e.g., the growth and stacking of the layers, the type of intercalated anions, and, accordingly, their catalytic activity in the isomerization of glucose into fructose. Serhal et al. (Serhal et al. 2018) suggested an ultraquick synthesis of hydrotalcite-like compounds which leads to an open Mg–Co/Al–Fe hydrotalcite structure and calcined samples show an improvement in the catalytic activity toward the oxidation of propene.

Despite many achievements in the research of Guerbet condensation, catalytic ethanol upgrading still requires the development of more robust catalysts in terms of activity and selectivity. Thus, the major goal of this research is to improve the performance of catalysts for ethanol-to-1-butanol condensation. In this work, the higher performance of hydrotalcite-derived $MgO–Al_2O_3$ systems is achieved by the implementation of fast hydrotalcite precursor synthesis and, thus, redistribution of active acid–base sites on the surface.

Experiment

Catalyst preparation

Mg–Al hydrotalcites with Mg/Al atomic ratios of 2 and 3 denoted as Mg–Al-2 and Mg–Al-3, respectively, were obtained by coprecipitation under high super saturation at pH 10–12. 1 M solutions of $Mg(NO_3)_2{\cdot}6H_2O$ and $Al(NO_3)_3{\cdot}9H_2O$ in various proportions were dropped into a buffer solution containing 1.6 M NaOH and 0.1 M Na_2CO_3 under vigorous stirring at a temperature of 358 K. For the preparation of Mg–Al-2 and Mg–Al-3 samples, the mixture was kept at 358 K for 24 h. For the Mg–Al-2-Fast and Mg–Al-3-Fast samples, the mixture was kept only for 1 h at identical conditions. Afterward, all precipitated solids were separated by a hot filtration, washed several times with warm deionized water until neutral pH was reached, and dried at 393 K for 6 h. The resulting hydrotalcites were thermally treated at 873 K for 5 h to obtain mixed oxides.

Catalyst characterization

XRD patterns of the powder samples were recorded using a D8 Advance (Bruker AXS GmbH, Germany) diffractometer with Cu-Kα radiation (nickel filter, $\lambda = 0.154$ nm).

The morphology of the samples was examined by means of scanning electron microscopy (SEM) using a Tescan MIRA 3 microscope operating at 30 keV electron beam energy with an In-beam SE (Secondary Electrons) detector. Chemical composition mapping analysis was carried out using energy dispersive X-ray spectroscopy (EDX) with a Bruker XFlash detector mounted directly into the SEM.

Textural properties of the powder samples were determined by low-temperature (77 K) nitrogen ad(de)sorption measured with a Sorptomatic-1990 porous analyser. Before measurements, the samples were evacuated at 473 K for 2 h. The specific surface area of the samples was determined by the Brunauer–Emmett–Teller (BET) method. External surface area and micropore volume

of the investigated samples were estimated from t-plot method. The mesopore size of the samples was obtained by the Barrett–Joyner–Halenda (BJH) method.

^{27}Al solid-state magic-angle spinning (MAS) nuclear magnetic resonance (NMR) experiments were carried out on an Agilent Technologies VNMRS 600 MHz spectrometer (14.1 Tesla 51 mm bore Oxford superconducting magnet) operating at a ^{27}Al Larmor frequency of 156.4 MHz, and using a 3.2 mm MAS probe head. The spectra were recorded using a single pulse acquisition with small pulse angle ($\pi/12$), at a spinning speed of 20 kHz and with a recycle delay of 4 s. All measurements were carried out at room temperature employing $AlCl_3{\cdot}6H_2O$ as a standard reference (0 ppm). All spectra were normalized to the same area under the curves.

In situ ^{27}Al liquid-state NMR investigation during the synthesis of Mg–Al hydrotalcites was held using an Avance 400 MHz spectrometer (Bruker) operating at a ^{27}Al Larmor frequency of 156.4 MHz. All measurements were carried out at room temperature employing $Al(NO_3)_3$ water solution as a standard reference (0 ppm). The mother liquor together with the precipitated hydrotalcite was sampled for 1 h from the beginning of the synthesis with an interval of 5 min, and the final sample was taken after 24 h of keeping the precipitate.

Acid–base characteristics of the samples were studied by NH_3 and CO_2 temperature-programmed desorption (TPD) using an Altamira AMI 300lite catalyst characterization system equipped with a thermal conductivity detector. The sample weight for the measurements was 0.1 g. Before adsorption of NH_3 and CO_2, the samples were heated in a constant He flow (20 ml/min) at 873 K for 1 h, then cooled in He flow to 373 K. Adsorption of NH_3 and CO_2 was carried out using a gaseous solution of NH_3 and CO_2 in Ar (at a flow rate of 20 ml/min) for 30 min. Then, the physically adsorbed molecules were removed by purging in a helium stream (flow rate of 20 ml/min) for 40 min. The following desorption was carried out by raising the temperature to 873 K with a heating rate of 10 K/min. The concentration of acid and base sites ($\mu mol/g_{cat}$) was determined from the amount of NH_3 and CO_2 adsorbed on the sample surface at a certain temperature. The integrated areas of the overlapping features in the TPD spectra were calculated after deconvolution of the recorded patterns by means of an Origin program, employing a Gaussian function to fit the experimental peak shape. The desorption temperature of the probe molecule was used as a criterion for the strength of acid/base sites.

Catalytic activity measurement

Catalytic activity tests were carried out in a fixed-bed flow quartz reactor with an inner diameter of 10 mm at 548–598 K and under atmospheric pressure. Samples with grains of 0.25–0.5 mm were loaded into the reactor. Ethanol (95.6 vol%, H_2O is the rest) feed was introduced to the evaporator via a syringe infusion pump. Ar was used as the carrier gas with a flow of 10 mL min^{-1}. The reaction was carried out at weight hourly space velocities (WHSV) of 0.14−0.56 g g_{cat}^{-1} h^{-1}. Before catalytic tests, samples were annealed in Ar at 773 K for 1 h. The reagents and reaction products were analysed on a gas chromatograph (NeoCHROM, Ukraine) equipped with an FID detector and a capillary column (HP-FFAP, 50 m × 0.32 mm).

Catalytic activity regeneration experiment was carried out for the Mg–Al-2 sample. Initially, catalytic experiment was held at 548 K according to the abovementioned procedure and continued for 2 h. After that, the catalyst was annealed at 773 K in air flow for 30 min to remove the carbon deposits on the surface and return high activity. After this, the temperature was set to 548 K again for 2 h and 5 cycles of ethanol-to-1-butanol condensation was performed.

Catalytic activity of the catalysts was characterized by conversion (X_{EtOH}):

$$X_{EtOH} = \frac{n^0_{EtOH} - n_{EtOH}}{n^0_{EtOH}} \cdot 100\%,$$

where n^0_{EtOH} is the initial amount of C moles of ethanol in the feed; n_{EtOH} is the amount of C moles of the unreacted alcohol in the stream of the reaction products:

$$n = C \cdot F,$$

where C is molar concentration of the component in the stream (mol L^{-1}), F is a flow rate of the stream (L h^{-1}).

Selectivity to products (S) and yield (Y) were calculated by the following formulas:

$$S_i = \frac{n_i}{(n^0_{EtOH} - n_{EtOH})} \cdot 100\%,$$

$$Y_i = \frac{X_{EtOH} \cdot S_i}{100\%},$$

where n_i is the amount of C moles of identified carbon-containing product. The main detected products are 1-butanol, 1-hexanol (HeOH), acetaldehyde (AA), ethylene (Et), diethyl ether (DEE). "Light" is the sum of acetone, ethyl acetate, 1-butene, 1-butanal, 1,3-butadiene and other light fractions. "Heavy" is the other condensation products: alcohols, namely, 2-ethyl-1-butanol, 2-ethyl-1-hexanol and 1-octanol, aldehydes, ketones, aromatics.

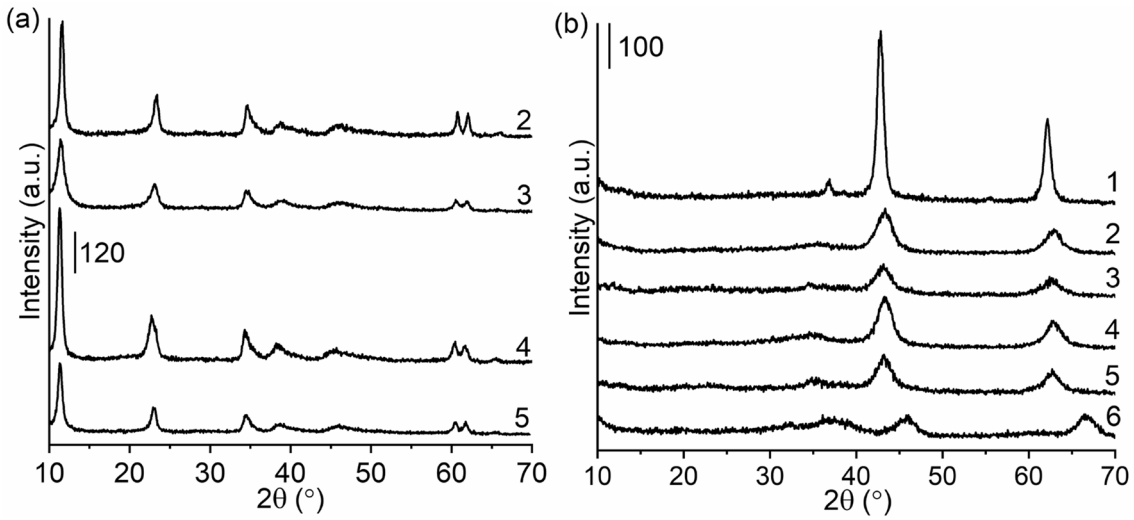

Fig. 1 XRD patterns of the dried at 393 K hydrotalcites (**a**) and after treatment at 873 K (**b**) 1—MgO, 2—Mg–Al-2, 3—Mg–Al-2-Fast, 4—Mg–Al-3, 5—Mg–Al-3-Fast, 6—Al_2O_3

Results and discussion

Structural and textural characteristics

Figure 1 shows powder X-ray patterns of the samples obtained by coprecipitation and standard X-ray patterns of Al_2O_3 and MgO. The diffractograms of synthesized hydrotalcite precursors (Fig. 1a) exhibit a series of sharp reflections for the 11.5° (0 0 3), 23.3° (0 0 6), 34.6° (0 0 9), 60.7° (1 1 0), 62.0° (1 1 3) planes and broadened signals for the 38.7° (0 1 5), 46.0° (0 1 8) planes. Such crystalline structure is identified as hydrotalcite, which consists of layered double Mg–Al hydroxides with brucite-like layers (Cantrell et al. 2005). According to the XRD results, the variation in the hydrotalcite crystallinity is found. As the amount of aluminium in the Mg–Al-3 is lower than in Mg–Al-2, the crystalline peaks are sharper and more intense, which is connected with higher crystalline perfection of stoichiometric $Mg_6Al_2CO_3(OH)_{16}{\cdot}4H_2O$ hydrotalcite. The same tendency is observed for the fast synthesized samples, which possess more crystallinity compared samples made by a standard method.

Figure 1b shows the XRD patterns after calcination of the samples at 873 K. The weak broad diffraction peaks at 35°, 43°, and 63° reveal the formation of Mg–Al mixed oxides which are actually $Mg(Al^{3+})O$ solid solutions of MgO-periclase type with planes (1 1 1), (2 0 0), (2 2 0) (MacKenzie et al. 1993; Gennequin et al. 2010). During the calcination of Mg–Al hydrotalcite, the Al^{3+} ions go out of octahedral layers into the interlayer space, forming spinel-like octahedral–tetrahedral layers (Díez et al. 2003). The formation of crystal $MgAl_2O_4$ phase is not obvious, since the main lines of spinel species can be hidden under the major MgO phase reflections if small amounts are present in the samples. Thus, a high dispersion of Mg and Al is detected and the sample crystallinity is increased with the rising of hydrotalcite aging time.

The SEM micrographs of the Mg–Al oxide systems (Fig. 2) show a well-developed layered structure. Mg–Al oxide samples are formed by quite similar aggregates, but with different sizes. The Mg–Al-2 sample possesses a well-developed platelet structure typical for layered materials. It is formed by aggregates consisting of thin plate-like crystals 80 – 150 nm in size. The micrographs of Mg–Al-2-Fast allow assuming the presence of an amorphous constituent in the sample (50 – 100 nm). The images of Mg–Al-3 depict the highest crystallinity between the samples under study 100 – 150 nm. In turn, Mg–Al-3-Fast is composed of plate-like crystals which are smaller in size (80 – 120 nm). One can notice that both Al content and the preparation time influence the particle size and morphology which is in line with XRD analysis. EDX elemental mapping images and EDX spectra (Figures S1 and S2 in Online Resource) indicate the uniform distribution of magnesium and aluminium in the sample, and confirm the absence of sodium in the sample composition as preparation residues.

Analysis of the results of nitrogen ad(-de)sorption measurements (Table 1, Fig. 3) shows that the studied Mg–Al-oxide systems are characterized by a relatively close total surface area (S_{BET}: 190–230 m^2/g) and are mainly mesoporous materials ($V_{me} = 0.41-0.73$ cm^3/g) with an average pore diameter in the range of 20–40 nm. The Mg–Al-2-Fast and Mg–Al-3-Fast samples are characterized by higher porosity, compared to the samples prepared by the standard method. The formation of a porous structure with higher values of volume and specific surface

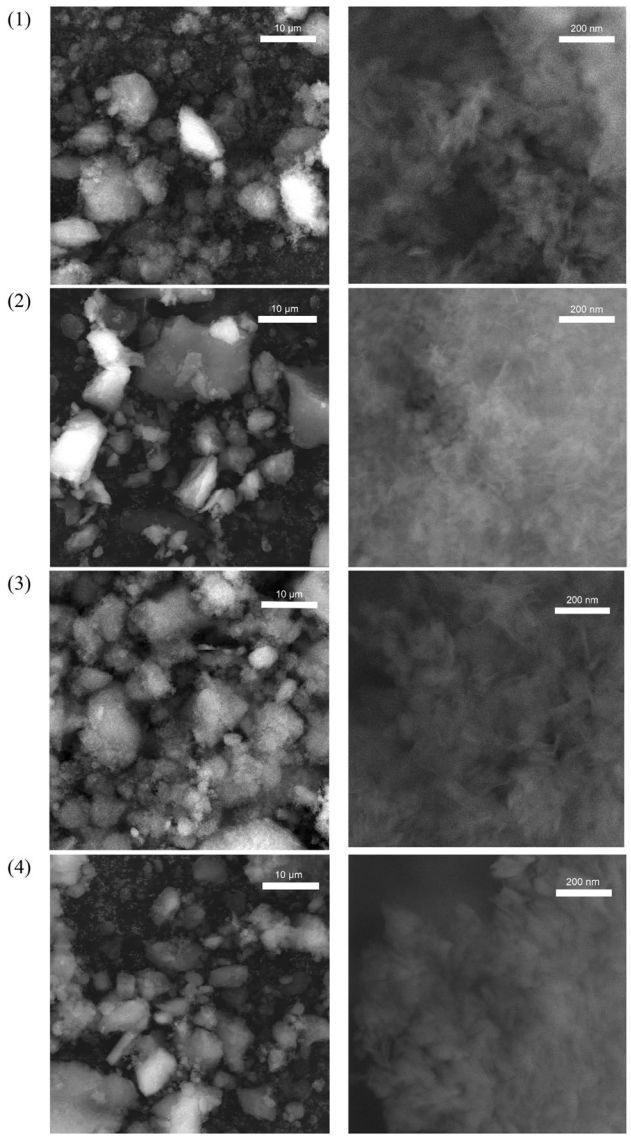

Fig. 2 SEM images of the samples after a treatment at 873 K: 1—Mg–Al-2, 2—Mg–Al-2-Fast, 3—Mg–Al-3, 4—Mg–Al-3-Fast

of micro-, supermicro- and mesopores of the samples was observed. The tendency to increase in these parameters of the mesoporous structure is more pronounced for the systems with a ratio of Mg/Al = 2:1 compared to Mg/Al = 3:1, which is manifested in the isotherms as the increase in adsorption at medium relative pressures (Fig. 3). In addition, total mesopore and external surface area, $S_{me} + S_{ext}$, are drastically increasing: 2 times for Mg–Al-2-Fast and 1.5 times for Mg–Al-3-Fast.

A detailed analysis of the porous structure parameters (Fig. 4) of the synthesized Mg–Al oxides shows that their mesoporous structure is formed at the step of precipitation of the corresponding hydrotalcites, namely, the fast method (within 1 h) increases the homogeneity of micro- and mesoporous structure. A significant increase in the precipitation time (up to 24 h) of hydrotalcites leads to hydrothermal aging of the hydrotalcites and the corresponding changes in the parameters of the porous structure of the resulting Mg–Al oxides. Increasing the amount of magnesium hydroxide in hydrotalcites promotes more intensive hydrothermal aging and reduces the volume and homogeneity of the porous structure in the resulting oxides.

As can be seen from in situ ^{27}Al liquid-state NMR spectra of the mother liquor sampled during the hydrotalcite synthesis (Fig. 5), the ones for Mg–Al-2 and Mg–Al-3 are quite similar and contain broad signal oriented at ~ 70 ppm. Basically, it indicates the presence of predominantly tetrahedrally coordinated aluminium, which formation is favoured at pH > 7 (Sivakumar and Emamjomeh 2005). The additional sharp signal at 80 ppm was detected from 10 to 50 min of the synthesis. It refers to the tetrahedral monomers $Al(OH)_4^-$ present in the aluminium aqueous solutions under the condition of high alkalinity (Perry and Shafran 2001). In addition, under the given condition the formation of the Keggin isomers, which have central metals tetrahedrally coordinated to oxygens, i.e., $Al(O)_4$ sites, is possible (Casey et al. 2001). The broad main signal in the AlO_4 chemical shift range could be the superposition of other different signals: ε-Al_{13} (63 ppm), Keggin aluminium polycations having a central AlO_4 in a shell of AlO_6 (63 ppm), Al_{30} (70 ppm), chain-ending singly connected Al (75 ppm), γ-Al_{13} (76 ppm), $Al_2O(OH)_6^{2-}$ dimers (78 ppm) (Shafran and Perry 2005; Martineau et al. 2016). The asymmetry of ^{27}Al NMR signal to the side of lower 20–0 ppm could indicate the presence of $Al(O)_6$ octahedral oligomers organized into cubane-like moieties that are linked together in a structure similar to the mineral brucite $Mg(OH)_2$ (Casey 2006). For the hydrotalcites washed from the mother liquor, the tetrahedral structure is preserved, which can occur due to the intercalation of $Al(OH)_4^-$ hydroxyaluminate anions between the Mg–Al double hydroxide layers (Xu and Lu 2005). Whereas the dried hydrotalcites are usually characterized exclusively by octahedrally coordinated aluminium (Occelli et al. 2003).

^{27}Al solid-state MAS NMR measurement of the samples after treatment at 873 K has been performed to identify the nature of alumina species (Fig. 6). Two signals of aluminium cations are observed in the spectra: one refers to Al^{3+} tetrahedrally coordinated with oxygen (Al_{tetra}, $\delta = 68-83$ ppm), and the other can be attributed to Al^{3+} octahedrally coordinated with oxygen (Al_{octa}, $\delta = 11-18$ ppm). In turn, each of the signals consists of two components. Lines at $\delta = 16-18$ and 79−83 ppm can be classified as octahedrally and tetrahedrally coordinated aluminium cations of the highly dispersed phase with [Mg–O–Al] bonds. Lines at $\delta = 11$ and 69 ppm can be

Table 1 Textural characteristics (nitrogen ad(de)sorption, 77 K) of Mg–Al oxide systems

Sample	S_{BET}[1], m^2/g	$S_{me}+S_{ext}$[2], m^2/g	V_{Σ}[3], cm^3/g	$(V_{mi}+V_{s\text{-}mi})$[4], cm^3/g	V_{me}[5], cm^3/g	$D_{me,max}$[6], nm	$D_{me,mean}$[7], nm
Mg–Al-2	230	75	0.48	0.07	0.41	45 ± 22	36
Mg–Al-2-Fast	225	165	0.77	0.04	0.73	21 ± 7	20
Mg–Al-3	190	100	0.67	0.06	0.61	27 ± 10	40
Mg–Al-3-Fast	215	150	0.75	0.03	0.72	17 ± 8.5	25

[1]Total surface area calculated using BET method

[2]Total mesopore and external surface area calculated using t-plot method

[3]Total pore volume at $p/p_0 = 1.0$

[4]Micro- and supermicropore volume calculated using t-plot method

[5]Mesopore volume calculated using t-plot method

[6]Maximal mesopore dimeters calculated using the Barrett–Joyner–Halenda method

[7]Median mesopore dimeters calculated using the Barrett–Joyner–Halenda method

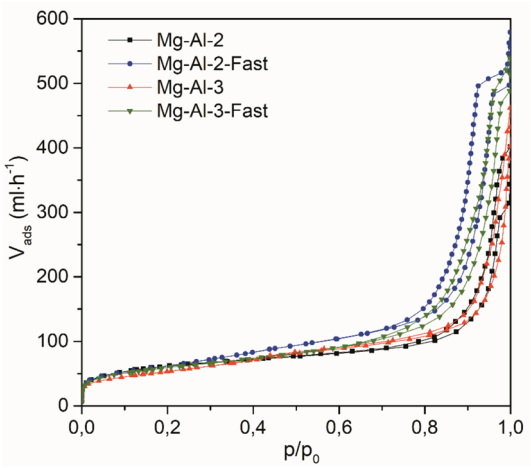

Fig. 3 Nitrogen adsorption/desorption isotherms for the prepared Mg–Al oxide systems

attributed to γ-alumina as an individual phase with bonds [Al–O–Al] (Larina et al. 2019). It should be noted that the samples with the ratio Mg/Al = 3 contain a larger proportion of the individual phase γ-Al_2O_3 compared to Mg/Al = 2.

Thus, the implementation of the fast preparation method allows to obtain hydrotalcite-derived Mg–Al oxide systems that differ from those synthesized by the standard procedure mainly in textural characteristics given by the reduced time for sediment aging. The time of synthesis affects more on the porous structure, but not the phase composition and structural characteristics.

Acid–base properties

Figure 7 shows the distribution profiles of acid and base sites on desorption temperature of NH_3 and CO_2, which characterizes a strength of acid/base sites over the surface of Mg–Al oxide systems. Acid and base sites were assigned as four groups depending on desorption temperature: < 473 K—weak, 473−573 K—moderate-weak, 573−723 K—moderate-strong, and > 723 K—strong sites. Table 2 represents the data on acid–base characteristics of the sites, obtained from the deconvolution of NH_3-TPD and CO_2-TPD spectra of the Mg–Al oxides.

As we can see, the Mg–Al-2, Mg–Al-2-Fast and Mg–Al-3-Fast samples possess quite similar distribution by strength and concentration of acid sites, i.e., 255, 262 and 243 μmol NH_3/g, respectively. On the contrary, the Mg–Al-3 sample demonstrates the highest concentration of acid surface sites of 394 μmol NH_3/g and more than two times higher capacity of (moderate-strong + strong) acid sites than other samples. Such tendency of much higher acidity of the Mg–Al-oxide system with the ratio of Mg/Al = 3, synthesized by the standard method was also observed in the previous work (Larina et al. 2019). The implementation of the fast hydrotalcite synthesis leads to decrease in total acidity of the Mg–Al oxide system with the ratio of Mg/Al = 3 due to the formation of a lower number of moderate-strong acid sites and slightly affects the acidity of Mg–Al oxide with Mg/Al = 2. Capacity ratio of (weak + moderate-weak)/(moderate-strong + strong acid sites) changes in a sequence:

$$\mathrm{Mg{-}Al{-}2-3.0} > \mathrm{Mg{-}Al{-}3{-}Fast-2.5} > \mathrm{Mg{-}Al{-}2{-}Fast-2.4} > \mathrm{Mg{-}Al{-}3-1.3}.$$

The Mg–Al-3 and Mg–Al-2 samples were studied by FT-IR spectroscopy with adsorbed pyridine earlier (Larina et al. 2019). The bands characteristic of pyridine adsorption

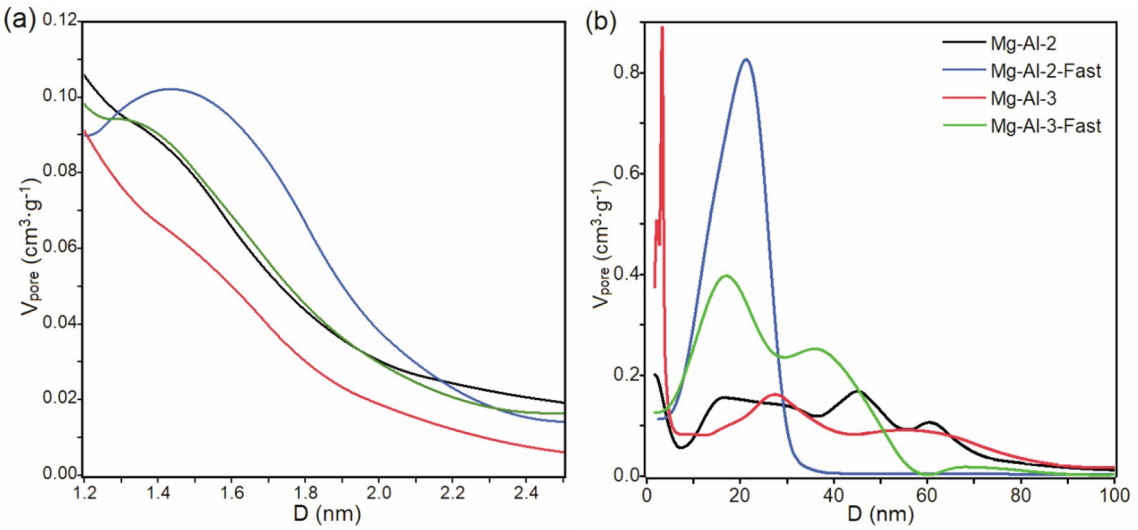

Fig. 4 Pore size distribution for the Mg–Al oxide systems: microspores (**a**), mesopores (**b**)

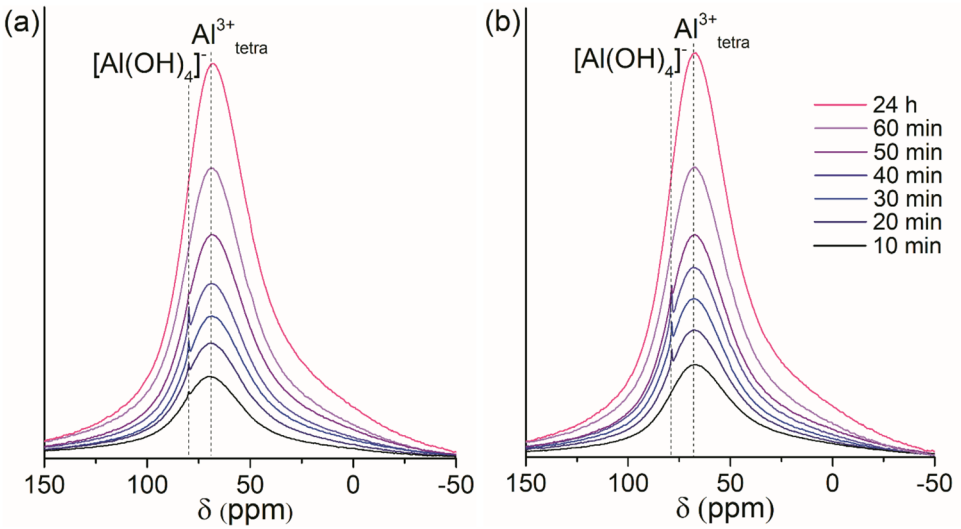

Fig. 5 In situ ^{27}Al liquid-state NMR spectra of the mother liquor sampled during the hydrotalcite synthesis: a—Mg–Al-2, b—Mg–Al-3

on Brønsted acid sites are not detected in the spectra. There are Lewis acidic sites on the surface only.

The different tendency has been found for the total concentration of base sites on Mg–Al oxide surface. For the samples with the Mg/Al ratio of 2 the concentration of base sites decreased from 185 to 169 μmol CO_2/g using the fast method of hydrotalcite preparation. On the contrary for the systems with the Mg/Al ratio of 3 the concentration increased from 215 to 233 μmol CO_2/g. However, the important dependence should be noticed, that the implementation of the fast hydrotalcite synthesis leads to a drastic increase in total concentration of (weak + moderate-weak) base sites: from 61 to 122 μmol CO_2/g for Mg/Al = 2, and from 77 to 129 μmol CO_2/g for Mg/Al = 3, with a noticeable decrease in total concentration of (moderate-strong + strong) base sites on the surface. Capacity ratio of (weak + moderate-weak)/(moderate-strong + strong) base sites varies in a next sequence:

$$\mathrm{Mg{-}Al{-}2{-}Fast} - 1.2 = \mathrm{Mg{-}Al{-}3{-}Fast} - 1.2 > \mathrm{Mg{-}Al{-}3} - 0.6 > \mathrm{Mg{-}Al{-}2} - 0.5.$$

According to the results of previous investigations (Larina et al. 2019, 2021b), the acid/base capacity ratio is determined as an important characteristic of the activity and selectivity of Mg–Al oxide catalysts. The acid/base capacity ratio (ABCR) for the studied samples varies in a sequence, having the lowest value of 1.0 for the Mg–Al-3-Fast sample (Table 2):

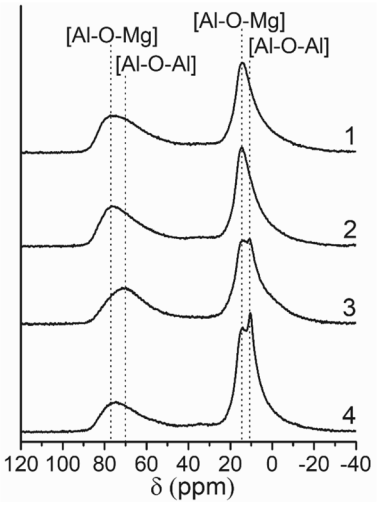

Fig. 6 ^{27}Al solid-state MAS NMR spectra of the samples: 1—Mg–Al-2, 2—Mg–Al-2-Fast, 3—Mg–Al-3, 4—Mg–Al-3-Fast

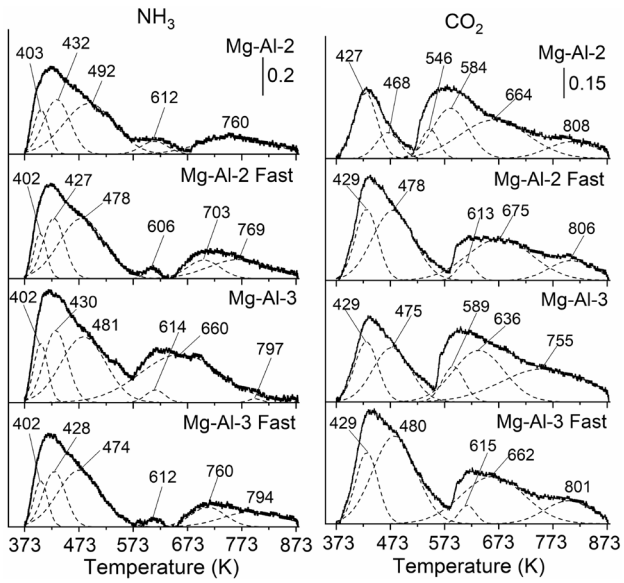

Fig. 7 Normalized to the same sample weight NH_3 and CO_2 temperature-programmed desorption profiles and the corresponding fit for the Mg–Al oxide systems: 1—Mg–Al-2, 2—Mg–Al-2-Fast, 3—Mg–Al-3, 4—Mg–Al-3-Fast

$$\mathrm{Mg{-}Al{-}3-1.8} > \mathrm{Mg{-}Al{-}2-1.4} > \mathrm{Mg{-}Al{-}2{-}Fast-1.3} > \mathrm{Mg{-}Al{-}3{-}Fast-1.0}.$$

Catalytic properties

The catalytic properties of Mg–Al oxide systems in vapour phase condensation of EtOH to BuOH in a flow mode are investigated at 548, 573 and 598 K. The dependences of EtOH conversion and product selectivity on time on stream (TOS) during 12 h are depicted in Figs. 8 and 9. Table S1 (Online Resource) represents the corresponding indices at 0.5, 3, 6 and 12 h TOS.

In the series of Mg–Al oxide catalysts, the initial EtOH conversion rises by 5−12% with an increase in the process temperature from 548 to 598 K as expected. At the same time, ethanol conversion on the catalyst samples prepared by the fast method is significantly higher than that achieved on the samples prepared by the standard method. Since the surface of Mg–Al-2 and Mg–Al-3 samples is dominated by strong and moderate-strong base sites, which are mainly represented by isolated O^{2-} anions, the condensation of ethanol can be inhibited at the step of intermediate carbanion formation during the dissociative adsorption of EtOH (Di Cosimo et al. 1998b). However, the increase in total surface area of mesopores and external surface due to the reduced time for sediment aging of hydrotalcite during the synthesis increases the accessibility of the base surface sites which, moreover, become somewhat weaker (Table 1).

Also, X_{EtOH} declines noticeably during the first 4 h on stream and then remains quite stable for the next 8 h except for the experiments at 548 K over Mg–Al-2-Fast and Mg–Al-3-Fast, where EtOH conversion decreases continuously down to 12 h (Figs. 8 and 9). The highest X_{EtOH} of 48% is achieved over Mg–Al-2-Fast at 598 K and 0.5 h TOS. At 598 K and TOS = 6 h, EtOH conversion for all samples has similar values of 19−22%. Herewith, BuOH selectivity decreases over Mg–Al-2 and Mg–Al-3 samples continuously during the 12 h TOS. The highest initial S_{BuOH} of 66% is reached over Mg–Al-2 at 548 K, but it is not stable in time. Similarly, the drop in the S_{BuOH} values reaches 20% in comparison with initial selectivity over Mg–Al-3 at 548 K (64% at 0.5 h and 44% at 12 h). In turn, Mg–Al-2-Fast and Mg–Al-3-Fast samples demonstrate stable BuOH selectivity with slight changes in time. Mg–Al-2-Fast demonstrates the highest S_{BuOH} of 64%, which remains on the same level till 12 h TOS.

The catalyst stability is a key issue in the long-term use of the catalyst in the EtOH-to-BuOH condensation process (Dias et al. 2014). It was reported previously (Di Cosimo et al. 1998a; León et al. 2011) that Mg–Al-oxides, which are characterized by quite high catalytic performance, can lose from 6% and even up to 50% of their activity after 8–10 h of operation in a flow mode. However, the mechanism of deactivation of these catalysts during the condensation of EtOH in BuOH still remains unclear.

Along with the direct condensation reaction with carbon chain doubling, a number of side reactions also occur. The more common side reactions include dehydration of olefins or ethers, esterification, oxidation to carboxylic acids, or subsequent aldol condensation (Gabriëls et al. 2015).

Table 2 Acid–base characteristics of the studied Mg–Al oxide systems

Characteristics	Temperature of desorption peak maxima of NH_3 and CO_2	Samples			
		Mg–Al-2	Mg–Al-2-Fast	Mg–Al-3	Mg–Al-3-Fast
Concentration of acid sites, μmol NH_3/g	< 473 K	27	23	33	25
		59	52	70	50
	473–573 K	105	110	121	99
	573–723 K	14	5	10	4
			24	159	27
	> 723 K	50	48	2	37
	Total	255	262	394	243
Concentration of base sites, μmol CO_2/g	< 473 K	35	40	31	38
		14			
	473–573 K	12	72	45	91
	573–723 K	42	8	17	7
		62	67	58	71
	> 723 K	20	22	62	26
	Total	185	169	215	233
Acid–base capacity ratio		1.4	1.3	1.8	1.0
Capacity ratio of (weak + moderate-weak)/(moderate-strong + strong acid sites)		3.0	2.4	1.3	2.5
Capacity ratio of (weak + moderate-weak)/(moderate-strong + strong base sites)		0.5	1.2	0.6	1.2

As a result of self- or cross-condensation of acetaldehyde and acetone, long-chain unsaturated aldehydes/ketones can be formed, which, through the course of the cyclization reaction, can form 2,4-dimethylbenzaldehyde molecules by gradually covering the active sites and causing catalyst deactivation (Yan et al. 2018). The work (Zhang et al. 2018) showed the deactivation of the ZnO/ZrO_2–SiO_2 catalyst in ethanol condensation into 1,3-butadiene due to the deposition of amorphous or even graphitized carbon formed by the destruction of aliphatic hydrocarbons. This led to a decrease in the catalyst activity due to a change in the parameters of the porous structure and blocking of acid surface sites. Moreover, H_2O formed during the Guerbet condensation reaction and ethanol dehydration could block the active sites of aldol condensation of acetaldehyde (Larina et al. 2021a).

The selectivity for 1-hexanol and "Heavy" products on the studied Mg–Al oxide catalysts decreases during the time on stream (Figs. 8 and 9). HeOH is formed when BuOH reacts with EtOH via Guerbet condensation and "Heavy" products are formed in parallel and subsequent condensation reaction of the alcohols. The sites being active in the condensation reaction are assumed to become blocked by adsorbed high-molecular condensation products, and this provokes their deactivation. Moreover, the unreacted acetaldehyde is raised in the products stream during the 12 h TOS on the studied samples. On the Mg–Al-3 catalyst, the AA formation is the most favourable among other catalysts and the selectivity reaches 25% at 548 K and TOS = 12 h.

DEE is more preferable dehydration product under the reaction conditions than Et and its selectivity increases with the rising of TOS. Mg–Al-3-Fast is more selective toward DEE among other systems and S_{DEE} reaches 19% at 598 K and TOS = 12 h. Selectivity toward the "Light" side products remains relatively stable during 12 h TOS for Mg–Al oxide catalysts. Only traces of crotonaldehyde are detected, meaning the step of crotonaldehyde hydrogenation occurs rapidly. Considering the noticeable decrease in EtOH conversion during the reaction only the initial BuOH yield reaches high values. The highest initial Y_{BuOH} of 23.4% is achieved over Mg–Al-2-Fast at 548 K (0.5 h TOS) and the highest stable Y_{BuOH} of 10.0% is registered at 598 K (12 h TOS) over the same catalyst.

Figure 10 presents cross-polarized ^{13}C NMR studies of the spent Mg–Al-2 and Mg–Al-3 catalyst obtained after the EtOH-to-BuOH conversion at 573 K during 12 h TOS. Adsorbed ethanol ($\delta^{13}C = 57$ and 16 ppm (Yan et al. 2018)) are observed on the sample surface. In addition, in the ^{13}C CP MAS NMR spectra there are the signals due to carbon atoms in CH_3–C (12–22 ppm) and –CH_2–C or > CH–C alkyl groups (30–40 ppm), aromatic (133 ppm), olefinic (139–142 ppm) and heteroaromatic (147–158 ppm) compounds (Bonardet et al. 1995). The signals at 166 and 180 ppm reflects the presence of ester and acid compounds on the spent catalysts surface, e.g., acetic acid $\delta^{13}C = 178$ and 21 ppm (Gottlieb et al. 1997), which can be formed by direct oxidation of acetaldehyde with water vapor present in

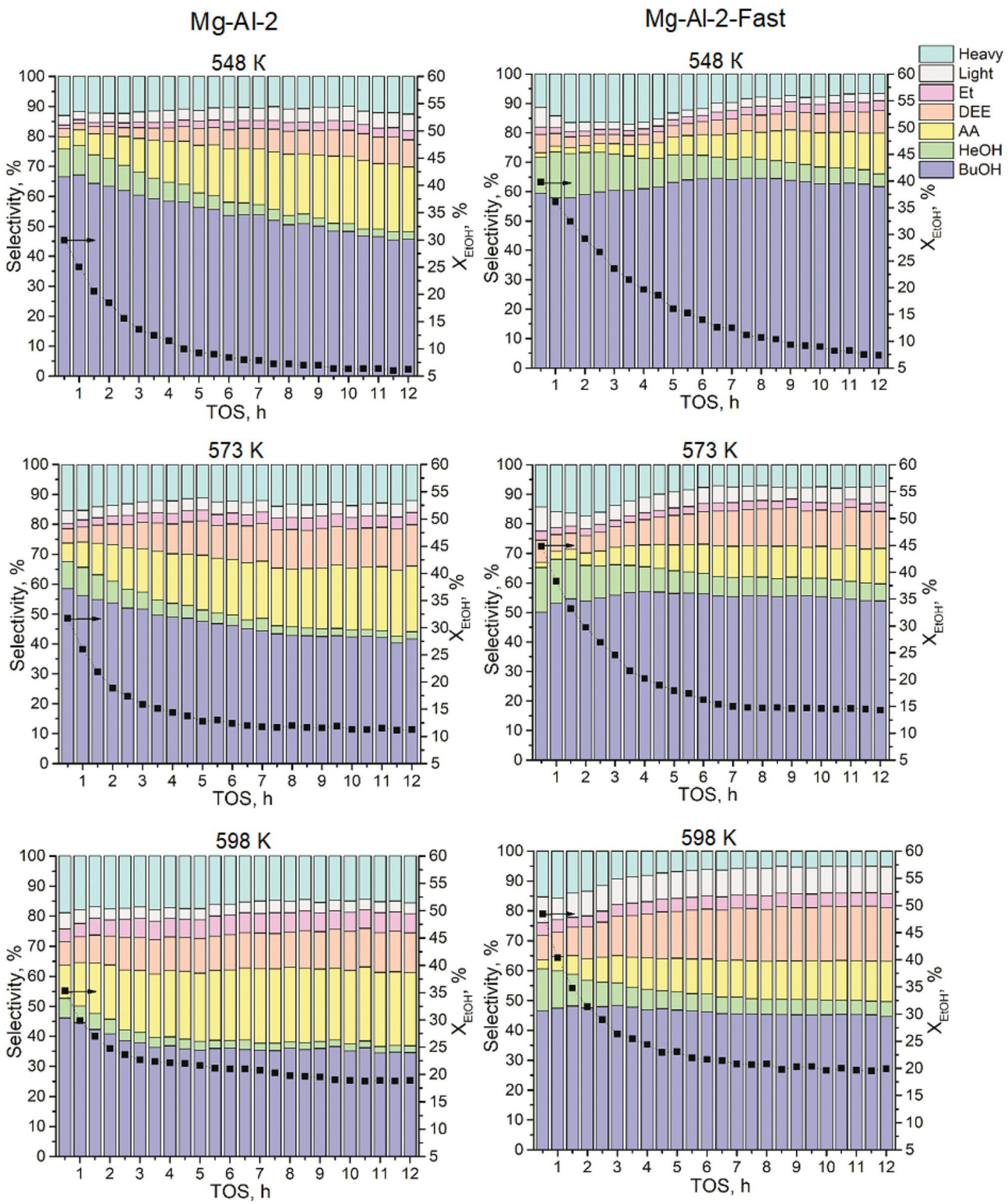

Fig. 8 Catalytic performance of Mg–Al-2 and Mg–Al-2-Fast samples in ethanol conversion in a flow mode during 12 h time on stream. Reaction condition: T = 548, 573 and 598 K, atmospheric pressure, WHSV = 0.14 g g_{cat}^{-1} h^{-1}

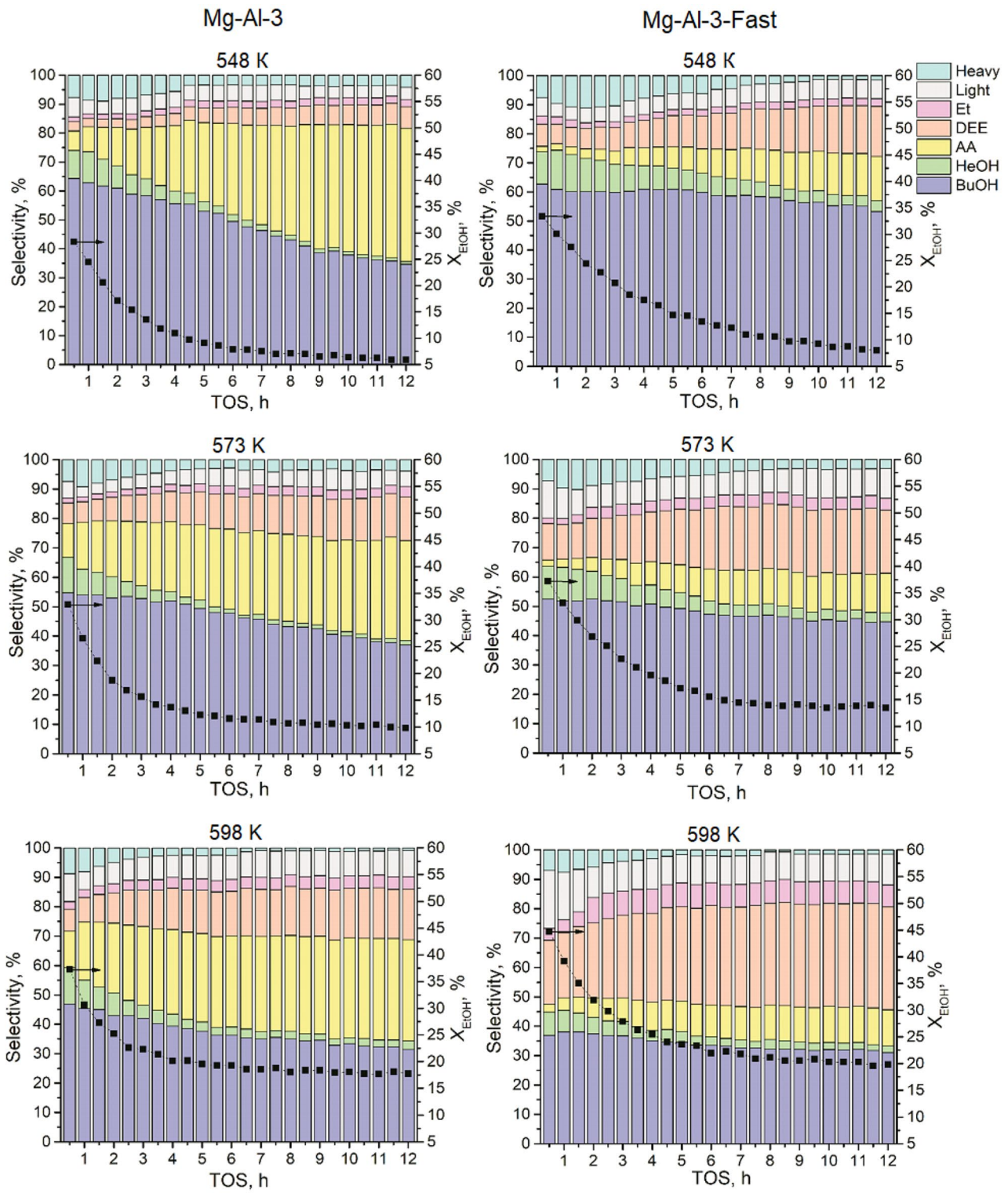

Fig. 9 Catalytic performance of Mg–Al-3 and Mg–Al-3-Fast samples in ethanol conversion in a flow mode during 12 h time on stream. Reaction condition: T = 548, 573 and 598 K, atmospheric pressure, WHSV = 0.14 g g_{cat}^{-1} h^{-1}

the reaction mixture. The signals of unsaturated aldehydes/ketones are absent, likely because these products are easily desorbed from the catalyst surface or aldol condensation stops at the aldol formation step. Therefore, cross-polarized ^{13}C NMR studies of the spent Mg–Al oxide catalyst samples confirm the aforementioned assumption that active aldol

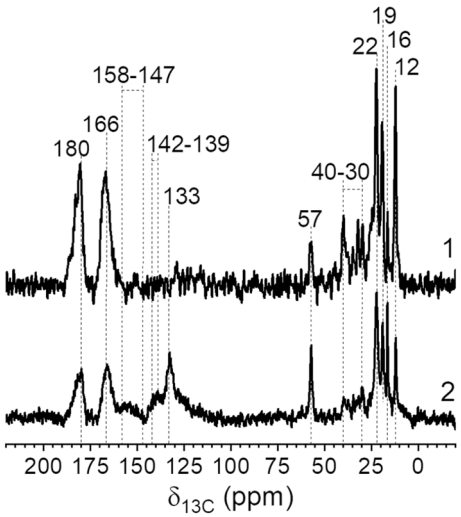

Fig. 10 ^{13}C CP MAS NMR spectra of the spent Mg–Al-2 and Mg–Al-3 catalyst (after the EtOH-to-BuOH conversion at 573 K during 12 h TOS)

condensation sites are blocked by adsorbed high-molecular condensation products, and this provokes their deactivation.

At close conversion values of ~ 8.5% and ~ 20%, the 1-butanol selectivity over Mg–Al-2-Fast is higher than over Mg–Al-2 (Table 3). At the same time for Mg–Al-2 and Mg–Al-3, a higher selectivity for AA is observed, which may indicate an insufficient number of active aldol condensation sites on the surface. In the presence of Mg–Al-2-Fast and Mg–Al-3-Fast samples, there is not only a lower selectivity for AA but also a lower selectivity for 1-hexanol and "Heavy" products. It can be assumed that a decrease in the sediment aging time of hydrotalcite during the synthesis causes the formation of active (base) sites of a certain (moderate) strength, sufficient for the condensation of ethanol into 1-butanol, and not enough for further condensation of 1-butanol.

The acid/base capacity ratio could give an understanding of the influence of acid–base characteristics on the activity and selectivity of Mg–Al oxide catalysts (Larina et al. 2019, 2021b). However, Mg–Al-2 and Mg–Al-2-Fast samples have really close ABCR values, 1.4 and 1.3 (Table 2), and different catalytic behaviour in the Guerbet condensation of ethanol. Thus, a more specific characteristic is needed as the ratio of (weak + moderate-weak)/(moderate-strong + strong sites). For the base sites, this ratio clearly shows that Mg–Al-2-Fast and Mg–Al-3-Fast samples with higher value of 1.2 are much more active and selective in the target process than Mg–Al-2 and Mg–Al-3 catalysts with 0.5 and 0.6. As for the acid sites, it was not observed a big difference between Mg–Al-3 and other samples, but the diversity in catalytic properties was not so significant. It could mean that acidity has a lower impact on the reaction path than basicity.

It is also noteworthy that acid–base characteristics are not the only critical parameter influencing catalytic properties in the process of ethanol to 1-butanol condensation. The formation of pores of higher volume and specific surface of micro-, supermicro- and mesopores and the external surface of the samples is obviously promoting the activity of Mg–Al-2-Fast and Mg–Al-3-Fast catalysts in the process. The change in mesoporous structure parameters is more conspicuous for the systems with a ratio of Mg/Al = 2:1 compared to Mg/Al = 3:1, thus the Mg–Al-2-Fast catalyst demonstrates more advanced catalytic properties.

Mg–Al-2 catalyst has been investigated in the catalytic activity regeneration experiment. Figure 11 presents the EtOH-to-BuOH process indices (EtOH conversion, BuOH selectivity and yield) during operation at 548 K with the regeneration at 773 K in air flow for 30 min every 2 h. The obtained results show that such regeneration is enough to remove the carbon deposits on the surface and return high

Table 3 Indices of EtOH-to-BuOH process over Mg–Al oxide catalysts

Sample	WHSV, $g\ g_{cat}^{-1}\ h^{-1}$	X_{EtOH}, %	Selectivity, %						
			BuOH	HeOH	AA	Et	DEE	Light	Heavy
Mg–Al-2	0.56	8.5	59.1	7.0	18.6	0.6	1.4	1.9	11.4
Mg–Al-2-Fast	0.56	8.3	65.8	5.2	3.9	2.3	17.9	2.9	2.0
Mg–Al-3	0.28	8.5	72.7	6.2	6.6	1.2	5.7	5.5	2.1
Mg–Al-3-Fast	0.50	8.4	56.0	3.7	4.8	3.0	27.6	3.4	1.4
Mg–Al-2	0.14	23.0	51.0	10.7	9.6	0.9	0.7	2.8	24.4
Mg–Al-2-Fast	0.28	20.5	63.5	10.1	2.2	1.6	8.4	3.6	10.7
Mg–Al-3	0.14	22.6	61.0	9.4	9.9	1.7	3.0	9.3	5.8
Mg–Al-3-Fast	0.28	19.1	59.7	8.3	2.8	2.7	15.6	5.1	5.8

Data are presented at close ethanol conversion values of ~ 8.5% and 20% (calculated as average at 0.5–2 h time on stream, T = 548 K). The main detected products are BuOH—1-butanol, HeOH—1-hexanol, AA—acetaldehyde, Et—ethylene, DEE—diethyl ether, "Light"—sum of ethyl acetate, acetone, 1-butene, 1-butanal, 1,3-butadiene and other light fractions, "Heavy"—other heavier products like alcohols, aldehydes, ketones, aromatics

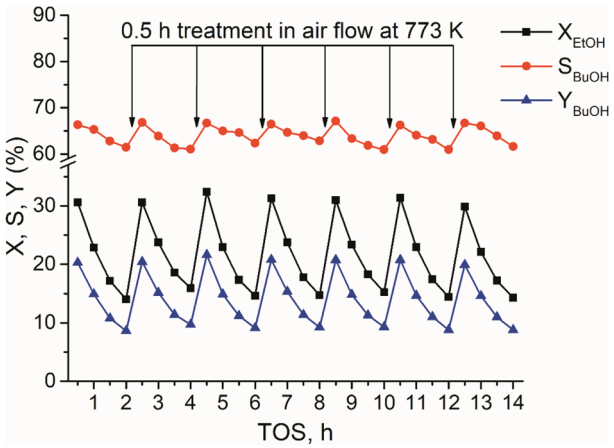

Fig. 11 Catalytic performance of Mg–Al-2 catalyst in ethanol conversion with impulse regeneration in air flow at 773 K. Reaction conditions: $T = 548$ K, atmospheric pressure, WHSV = 0.14 g g_{cat}^{-1} h^{-1}

catalyst activity. Therefore, the time of effective operation of Mg–Al-oxide catalysts in the process of vapor phase condensation of ethanol-to-1-butanol can be extended by periodically applying rapid regeneration in the reactor (in situ).

Conclusions

Hydrotalcite-derived Mg–Al oxide catalysts for vapour phase ethanol-to-1-butanol Guerbet condensation were synthesized and characterized using X-ray diffraction, scanning electron microscopy, ^{27}Al nuclear magnetic resonance, low-temperature (77 K) N_2 ad(de)sorption, and temperature-programmed desorption of NH_3 and CO_2. The implementation of the fast synthesis of hydrotalcite precursor for Mg–Al oxide systems gave the precious advantage in their catalytic characteristics. The increase in the volume of mesopores, total surface area of mesopores and external area, as well as the concentration of weak and moderate-weak base sites, increases the activity of catalysts and the selectivity of the formation of 1-butanol in the target process. It was found that the highest 1-butanol selectivity of 64% (stable till 12 h TOS) and yield of 23.4% is achieved over Mg–Al-2-Fast sample at 548 K. The obtained catalysts are reusable and their activity is sustainable after the repeated catalytic cycles. The robust efficiency for C–C coupling via the Guerbet reaction makes Mg–Al oxide systems obtained via fast synthesis a promising catalyst for 1-butanol production.

Supplementary Information The online version contains supplementary material available at https://doi.org/10.1007/s13204-023-02801-w.

Acknowledgements This work was financially supported by Project of research work of young scientists of the National Academy of Sciences of Ukraine "Design of modified Y–Mg–Si(Al) oxide catalysts for the production of important chemicals (1,3-butadiene, 1-butanol) from bioethanol" (0121U111813). The authors also acknowledge CERIC–ERIC Consortium for access to experimental facilities FE–SEM Surface and Plasma Science at Charles University in Prague (Proposal Number: 20192036) and financial support.

Data availability All data generated or analysed during this study are included in this published article (and its supplementary information files).

Declarations

Conflict of interest The authors declare no conflict of interest.

References

Birgen C, Dürre P, Preisig HA, Wentzel A (2019) Butanol production from lignocellulosic biomass: revisiting fermentation performance indicators with exploratory data analysis. Biotechnol Biofuels 12:1–15. https://doi.org/10.1186/s13068-019-1508-6

Bonardet JL, Barrage MC, Fraissard J (1995) Use of NMR techniques for studying deactivation of zeolites by coking. J Mol Catal A Chem 96:123–143. https://doi.org/10.1016/1381-1169(94)00030-1

Cantrell DG, Gillie LJ, Lee AF, Wilson K (2005) Structure-reactivity correlations in MgAl hydrotalcite catalysts for biodiesel synthesis. Appl Catal A Gen 287:183–190. https://doi.org/10.1016/j.apcata.2005.03.027

Casey WH (2006) Large aqueous aluminum hydroxide molecules. Chem Rev 106:1–16. https://doi.org/10.1021/cr040095d

Casey WH, Phillips BL, Furrer G (2001) Aqueous aluminum polynuclear complexes and nanoclusters: a review. Rev Min Geochem 44:167–190. https://doi.org/10.2138/rmg.2001.44.05

Choi H, Han J, Lee J (2021) Renewable butanol production via catalytic routes. Int J Environ Res Public Health. https://doi.org/10.3390/ijerph182211749

Choudhary P, Rao BAM, Mahaveer NS (2022) Butanol fuel in internal combustion engines. In: Application of clean fuels in combustion engines. Springer Nature Singapore, Print ISBN: 978-981-16-8750-1, Electronic ISBN: 978-981-16-8751-8. https://doi.org/10.1007/978-981-16-8751-8_6

da Trindade WRS, dos Santos RG (2017) Review on the characteristics of butanol, its production and use as fuel in internal combustion engines. Renew Sustain Energy Rev 69:642–651. https://doi.org/10.1016/j.rser.2016.11.213

Dai J, Zhang H (2019) Recent advances in selective C-C bond coupling for ethanol upgrading over balanced Lewis acid-base catalysts. Sci China Mater 62:1642–1654. https://doi.org/10.1007/s40843-019-9454-x

Daramola MO, Ayeni AO (2020) Valorization of biomass to value-added commodities, Springer International Publishing, Electronic ISBN 978-3-030-38032-8, Print ISBN 978-3-030-38031-1. https://doi.org/10.1007/978-3-030-38032-8

Di Cosimo JI, Díez VK, Xu M et al (1998a) Structure and surface and catalytic properties of Mg-Al basic oxides. J Catal 178:499–510

Di Cosimo JI, Díez VK, Xu M et al(1998b) Structure and surface and catalytic properties of Mg-Al basic oxides. J Catal 178:499–510. https://doi.org/10.1006/jcat.1998.2161

Dias MOS, Pereira LG, Junqueira TL et al (2014) Butanol production in a sugarcane biorefinery using ethanol as feedstock. Part I: Integration to a first generation sugarcane distillery. Chem Eng Res Des 92:1441–1451. https://doi.org/10.1016/j.cherd.2014.04.030

Díez VK, Apesteguía CR, Di Cosimo JI (2003) Effect of the chemical composition on the catalytic performance of MgyAlOxcatalysts for alcohol elimination reactions. J Catal 215:220–233. https://doi.org/10.1016/S0021-9517(03)00010-1

Gabriëls D, Hernández WY, Sels B et al (2015) Review of catalytic systems and thermodynamics for the Guerbet condensation reaction and challenges for biomass valorization. Catal Sci Technol 5:3876–3902. https://doi.org/10.1039/C5CY00359H

Gennequin C, Kouassi S, Tidahy L et al (2010) Co-Mg-Al oxides issued of hydrotalcite precursors for total oxidation of volatile organic compounds. Identification and toxicological impact of the by-products. Comptes Rendus Chim 13:494–501. https://doi.org/10.1016/j.crci.2010.01.001

Gottlieb HE, Kotlyar V, Nudelman A (1997) NMR chemicals shifts of common laboratory solvents as traces imputities. J Org Chem 62:7512–7515

Hahn H-D, Dämbkes G, Rupprich N et al (2013) Butanols. Ullmann's encyclopedia of industrial chemistry. Wiley-VCH Verlag GmbH & Co. KGaA, Weinheim

Larina OV, Valihura KV, Kyriienko PI et al (2019) Successive vapour phase Guerbet condensation of ethanol and 1-butanol over Mg-Al oxide catalysts in a flow reactor. Appl Catal A Gen 588:117265. https://doi.org/10.1016/J.APCATA.2019.117265

Larina OV, Kyriienko PI, Shcherban ND et al (2021a) Carbon-supported Mg–Al oxide hybrid catalysts for aqueous ethanol conversion into 1-Butanol in a flow reactor. Ind Eng Chem Res 60:11964–11976. https://doi.org/10.1021/acs.iecr.1c02153

Larina OV, Valihura KV, Kyriienko PI et al (2021b) Catalytic performance of ternary Mg-Al-Ce oxides for ethanol conversion into 1-butanol in a flow reactor. J Fuel Chem Technol 49:347–358. https://doi.org/10.1016/S1872-5813(21)60028-2

León M, Díaz E, Ordóñez S (2011) Ethanol catalytic condensation over Mg–Al mixed oxides derived from hydrotalcites. Catal Today 164:436–442. https://doi.org/10.1016/j.cattod.2010.10.003

Liu L, Climent M, Iborra S (2021) Biomass processing via metal catalysis. Biomass Valoriz. https://doi.org/10.1002/9783527825028.ch4

MacKenzie KJD, Meinhold RH, Sherriff BL, Xu Z (1993) 27Al and 25Mg solid-state magic-angle spinning nuclear magnetic resonance study of hydrotalcite and its thermal decomposition sequence. J Mater Chem 3:1263–1269. https://doi.org/10.1039/jm9930301263

Martineau C, Taulelle C, Haouas M (2016) The use of 27 Al NMR to study aluminum compounds: a survey of the last 25 years. PATAI's Chemistry of Functional Groups, John Wiley & Sons, pp 1–51. https://doi.org/10.1002/9780470682531.pat0840

Nair P, Meenakshi HN (2021) Review on the synthesis, performance and trends of butanol: a cleaner fuel additive for gasoline. Int J Ambient Energy. https://doi.org/10.1080/01430750.2021.1873849

Occelli ML, Olivier JP, Auroux A et al (2003) Basicity and porosity of a calcined hydrotalcite-type material from nitrogen porosimetry and adsorption microcalorimetry methods. Chem Mater 15:4231–4238. https://doi.org/10.1021/cm030105b

Park S, Kwon D, Kang JY, Jung JC (2019) Influence of the preparation method on the catalytic activity of Mg[sbnd]Al hydrotalcites as solid base catalysts. Green Energy Environ 4:287–292. https://doi.org/10.1016/j.gee.2018.11.003

Perry CC, Shafran KL (2001) The systematic study of aluminium speciation in medium concentrated aqueous solutions. J Inorg Biochem 87:115–124. https://doi.org/10.1016/S0162-0134(01)00326-9

Serhal CA, Mallard I, Poupin C et al (2018) Ultraquick synthesis of hydrotalcite-like compounds as efficient catalysts for the oxidation of volatile organic compounds. Comptes Rendus Chim 21:993–1000. https://doi.org/10.1016/j.crci.2018.09.012

Shafran KL, Perry CC (2005) A systematic investigation of aluminium ion speciation at high temperature. Part .1 solution studies. Dalt Trans. https://doi.org/10.1039/b502097b

Sivakumar M, Emamjomeh MM (2005) Electrochemical method for fluoride removal: measurement, speciation and mechanisms electrochemical method for fluoride removal: measurement, speciation, and mechanisms. Environ Postgr Conf Environ Chang Mak It Happen 61:1–8

Valihura KV, Larina OV, Kyriienko PI et al (2019) Effect of Composition of Mg-Al-Oxide systems on their catalytic properties in the production of 2-Ethyl-1-Hexanol in vapor-phase condensation of 1-Butanol in a flow system. Theor Exp Chem 55:337–344. https://doi.org/10.1007/s11237-019-09626-1

Wu X, Fang G, Tong Y et al (2018) Catalytic upgrading of ethanol to n-Butanol: progress in catalyst development. Chemsuschem 11:71–85. https://doi.org/10.1002/cssc.201701590

Wu Z, Wang P, Wang J, Tan T (2021) Guerbet reactions for biofuel production from abe fermentation using bifunctional ni-mgo-al2o3 catalysts. Catalysts. https://doi.org/10.3390/catal11040414

Xu Z, Lu G (2005) Hydrothermal synthesis of layered double hydroxides (LDHs) from mixed MgO and Al2O3: LDH formation mechanism. Chem Mater. https://doi.org/10.1021/cm048085g

Yan T, Yang L, Dai W et al (2018) On the deactivation mechanism of zeolite catalyst in ethanol to butadiene conversion. J Catal 367:7–15. https://doi.org/10.1016/j.jcat.2018.08.019

Zhang M, Tan X, Zhang T et al (2018) The deactivation of a ZnO doped ZrO2-SiO2 catalyst in the conversion of ethanol/acetaldehyde to 1,3-butadiene. RSC Adv 8:34069–34077. https://doi.org/10.1039/c8ra06757k